Research Square

Preprints are preliminary reports that have not undergone peer review.
They should not be considered conclusive, used to inform clinical practice,
or referenced by the media as validated information.

Covariance-Eigenvalue Analysis of Multichannel EEG for Structural Characterization and Subject-Independent Schizophrenia Detection

Ratheesh Sudheerbabu
Amrita Vishwa Vidyapeetham
Abhishek S
s_abhishek@cb.amrita.edu

Amrita Vishwa Vidyapeetham
Vinayakumar B
Middle East College

Article

Keywords:

Posted Date: November 12th, 2026

DOI: https://doi.org/10.21203/rs.3.rs-11483338/v1

License: This work is licensed under a Creative Commons Attribution 4.0 International License.
Read Full License

Additional Declarations: No competing interests reported.

Covariance-Eigenvalue Analysis of Multichannel EEG for Structural Characterization and Subject-Independent Schizophrenia Detection

Ratheesh Sudheerbabu[1], Abhishek S[1*], Vinayakumar B[2]

[1]Amrita School of Artificial Intelligence, Coimbatore, Amrita Vishwa Vidyapeetham, India.

[2]Department of Computing and Electronics Engineering, Middle East College, Knowledge Oasis Muscat, Oman.

*Corresponding author(s). E-mail(s): s_abhishek@cb.amrita.edu;
Contributing authors: s_ratheesh@cb.students.amrita.edu;
vinayakumar@mec.edu.om;

Abstract

This study investigates covariance-matrix eigenvalue representations as compact features for subject-independent schizophrenia classification using multichannel resting-state EEG. The analysis considers the covariance eigenvalue spectrum as a measure of the second-order arrangement of multichannel variance and evaluates it from many complimentary perspectives, including frequency, temporal, duration and structural elements. Five covariance-eigenvalue representations were created for frequency ranges of Delta (0.5-4 Hz), Theta (4-8 Hz), Alpha (8-13 Hz), Beta (13-30 Hz), and Gamma (30-45 Hz), resulting in 80 eigenvalue characteristics per participant. Comprehensive, standardized, condensed and subband representations were tested using thorough subject-level leave-one-subject-out (LOSO) cross-validation. The analysis also considered temporal instability, band-wise eigenvalue differences, and singular-value-decomposition-based measures of structural dimensionality. The last locked 10-s five-band covariance-eigenvalue model with XGBoost achieved an accuracy of 89.29%, a balanced accuracy of 88.97%, an ROC-AUC of 90.71%, a sensitivity of 93.33%, and a specificity of 84.62%. Statistical verification was conducted with subject-specific bootstrap confidence intervals and paired exact McNemar tests with Holm correction. After Holm correction, XGBoost showed substantial differences in paired prediction errors with SVM-RBF and kNN, but no statistically significant differences with Random Forest and Logistic Regression. Model interpretation was performed

using SHAP (SHapley Additive exPlanations). To assess whether dimensionality reduction could improve performance over the full 80-feature representation, nested SHAP/ANOVA-based feature-selection experiments and a localized sensitivity analysis for (K=55–65) features were conducted. Feature selection did not improve the primary LOSO accuracy (88.10% vs. 89.29%) or balanced accuracy (87.86% vs. 88.97%), although a modest increase in ROC-AUC was observed (0.9151 vs. 0.9071). The results of the study support the covariance-eigenvalue spectrum as a compact statistical model for subject-independent EEG assessment. However, independent-cohort validation is necessary before any clinical or biomarker claims can be made.

Keywords: EEG, schizophrenia, covariance matrix, eigenvalues, eigenspectrum, subband analysis, temporal stability, singular value decomposition, subject-independent classification, XGBoost.

1 Introduction

Schizophrenia is characterized by the presence of detectable neurological changes in brain electrical activity, and Electroencephalogram provides a non-invasive signal with exceptional temporal precision. Therefore, machine-learning techniques have been investigated to identify EEG patterns associated with schizophrenia from healthy controls. A perennial methodological challenge is that EEG recordings are high dimensional and show large inter-subject variability. Performance estimations may also be quite sensitive to how the temporal segments are split between training and test data. We consider an alternative representation, namely the eigenvalue spectrum of the multichannel EEG covariance matrix. Instead of using the covariance matrix simply as an intermediary step, we interpret the eigenvalues as a concise description of the distribution of signal variance over orthogonal channel-space modes. This leads to a mathematically well-defined representation that can be analyzed throughout frequency bands, recording periods, temporal segments, and cumulative explained-variance thresholds. The primary goal is thus not merely to maximize classification accuracy, but also to determine whether covariance-eigenvalue structure contains reproducible group-related information in a subject-independent evaluation. The study is based on four related questions: (1) do covariance eigenvalues contain discriminative information across frequency bands; (2) how does the representation change as a function of increasing recording duration; (3) is the temporal instability different for HC and SCZ; and (4) how does the covariance-eigenvalue structure relate to effective dimensionality derived through SVD. The motivation for this research arises from the necessity for a comprehensive and interpretable characterisation of schizophrenia- related changes in multichannel EEG, beyond conventional signal-level analysis and classification efficacy. Despite EEG recording intricate brain activity patterns, the degree to which its multichannel covariance structure demonstrates frequency-dependent, temporally evolving, and duration-sensitive alterations is insufficiently defined within a unified analytical model. This research systematically examines the eigenvalue spectrum of EEG covariance matrices across multiple frequency bands and recording durations, incorporating

statistical comparisons between healthy subjects and schizophrenia subjects, structural variability analysis, temporal and duration-dependent stability assessment, and subject-independent classification. The proposed framework attempts to clarify how schizophrenia-related differences are reflected in the distribution and organization of multichannel EEG covariance structures by linking interpretable spectral-spatial structural features with predictive performance, while evaluating the discriminative value and robustness of the resulting eigenvalue representations.

Figure 1 depicts the overall workflow for the proposed EEG-based schizophrenia classification framework. The framework starts with the MSU EEG dataset, which includes 84 subjects, 45 schizophrenia (SCZ) subjects, and 39 healthy controls (HC), with 16 EEG channels recorded at a sample frequency of 128 Hz. The raw EEG signals are first subjected to band-pass filtering (0.5–45 Hz), 50 Hz notch filtering, and amplitude normalization to reduce noise and signal variability. For each subject, the first 10-second EEG segment is chosen, which corresponds to 1280 samples per channel. The preprocessed signals are then decomposed into five conventional frequency bands: delta (0.5-4 Hz), theta (4-8 Hz), alpha (8-13 Hz), beta (13-30 Hz), and gamma (30-45 Hz). To characterize the spatial and functional correlations between EEG channels, a 16×16 covariance matrix is constructed for each frequency band, followed by eigenvalue decomposition. The 16 eigenvalues from each frequency band are combined to create an 80-dimensional five-band eigenvalue feature vector for each subject. These features are then fed into an optimized XGBoost classifier, which uses strict leave-one-out (LOSO) cross-validation to ensure subject independence and minimize potential data leakage. Finally, the framework generates a binary classification output that distinguishes healthy controls from schizophrenic subjects. This integrated frequency-specific covariance-eigenvalue representation, along with efficient machine learning, serves as the foundation for the proposed subject-independent schizophrenia classification framework.

1.1 Related works

Support vector machines (SVM), k-nearest neighbors (KNN), random forests (RF), decision trees (DT), logistic regression, linear discriminant analysis (LDA), Gaussian Naive Bayes, ensemble bagged trees, and quadratic discriminant analysis (QDA) are examples of classical machine learning techniques that have been extensively used for hand-crafted EEG features derived from time, frequency, and time–frequency domains. Concurrently, DL models have been proposed to directly learn hierarchical spatial-temporal representations from raw or minimally processed EEG [1]. These models include multilayer perceptrons (MLP), convolutional neural networks (CNN), recurrent and bidirectional LSTM architectures, GRU-based hybrids, region-based CNNs, and attention-driven or distributed activation networks [1–4]. To improve performance and robustness, hybrid frameworks like CNN+GRU, CNN–Transformer fusion pipelines, and CNN–ensemble tree combinations further used the combined benefits of strong classical classifiers and deep feature extraction.

The methodical use of several diverse EEG datasets to assess model generalizability across populations and settings is a crucial aspect of this research evolution.

The Kaggle schizophrenia EEG dataset (81 subjects, 32 healthy controls(HC), and 49 schizophrenia(SZ) patients , IBIB PAN/RepOD datasets (14 SZ and 14 HC), Zenodo ERP databases, adolescent cohorts with SZ symptoms, and institutional clinical datasets covering resting-state and task-based recordings have all been used in studies [4–11]. Cross-validation techniques, including 10-fold, leave-one-subject-out, and sometimes external validation [4], are employed in several research to show that suggested models maintain high accuracy across participants. Numerous studies have attained accuracy levels of 95%, and some have shown accuracy levels close to 100%.[12, 13]. The promise of EEG-based AI systems as reliable instruments for schizophrenia detection and monitoring is highlighted by this multi-dataset, well validated evidence base.

The literature's main themes are robustness, interpretability, and feature engineering. To capture both linear and nonlinear brain dynamics [14], traditional signal processing techniques like discrete wavelet transform (DWT) [15, 16], empirical mode decomposition (EMD) [17], empirical wavelet transform, multiresolution sub-band analysis [6], and power spectral density (PSD) estimation [18] are frequently combined with entropy and information-theoretic measures like multiscale fuzzy entropy, relative band power [19], correntropy, cross-information potential [12], and graph-theoretic connectivity indices (degree, clustering coefficient, local efficiency, robustness) [7]. These characteristics improve physiological interpretability in addition to driving high classification performance. For instance, they reveal improper entropy patterns or altered theta-band connections in bipolar disorder and schizophrenia [7, 12, 19]. Beyond conventional power-based analysis, eigenvector- and matrix-based representations provide related mathematical approaches for characterizing EEG signals. Bose et al.[20] investigated absolute EEG band power using Welch's PSD estimation and reported significant differences in Alpha- and Beta-band power between schizophrenia and healthy-control groups. Their findings support the relevance of frequency-specific EEG analysis, although PSD features are distinct from covariance-matrix eigenvalues. Earlier work by Übeyli [21] examined eigenvector-based spectral estimation methods, including Pisarenko, multiple signal classification (MUSIC), and the modified covariance method, for EEG feature extraction and neural-network classification. This work provides methodological context for the use of eigenvector-based signal representations, but addresses a different classification task from schizophrenia detection using subject-level covariance eigenspectra.

Beyond conventional spectral and statistical descriptors, previous studies have also investigated nonlinear EEG characteristics to capture the complex dynamics associated with neurological and psychiatric conditions. Related work has explored explainable analysis and complementary EEG feature representations to improve the interpretation of machine-learning predictions [22–24]. These studies motivate continued investigation of informative EEG representations that balance discriminative capability with interpretability. In this context, the present study examines covariance-eigenvalue spectra across frequency subbands, recording durations, and temporal segments, with SVD-derived measures providing an additional interpretation of multichannel variance organization. Unlike approaches that explicitly extract nonlinear features, the present framework focuses on covariance-based representations and their subject-independent evaluation.

Related studies have also represented multichannel EEG through connectivity matrices and graph-based methods. Bagherzadeh et al.[25] constructed transfer-entropy-based effective-connectivity images from multichannel EEG and used deep-learning models for schizophrenia classification. Pain et al.[26] proposed a graph signal processing and graph-learning framework that combines channel-level permutation-entropy features with learned interchannel relationships. These approaches emphasize interactions among EEG channels, whereas covariance-eigenvalue features summarize the distribution of multichannel variance across orthogonal modes. Although these representations are mathematically related through their use of matrices or spectral decompositions, they capture different properties of the signals and should not be treated as interchangeable. More recent studies have explored deep-learning approaches based on time–frequency representations, cross-dataset evaluation, and joint temporal–spatial dependency learning for schizophrenia detection [27, 28]. Collectively, this literature motivates investigating complementary representations of EEG signals while distinguishing conventional spectral power, effective connectivity, graph spectral features, and covariance-eigenvalue spectra.

Explainability and clinically relevant error reduction are also receiving increasing attention. Recent models incorporate attention mechanisms, distributed activation functions, multiview representations, and hybrid architectures to improve feature learning and model interpretation [2, 4]. Nevertheless, larger multicenter cohorts, standardized preprocessing and evaluation protocols, and transparent models remain necessary before clinical deployment can be justified [14]. Survey and review studies similarly emphasize the potential of EEG-based machine-learning and deep-learning frameworks for data-driven schizophrenia analysis, while highlighting the need for further validation [14, 29, 30].

Motivated by these developments, the present study investigates covariance-eigenvalue features derived from the MSU/MHRC EEG dataset. Rather than introducing an additional deep-learning architecture, it examines whether the eigenvalues of multichannel covariance matrices provide a compact representation of variance organization for subject-independent schizophrenia classification. The analysis extends this representation across five canonical EEG subbands and evaluates subband fusion, recording-duration effects, temporal eigenspectrum stability, and singular-value decomposition (SVD)-based spatial dimensionality. Feature-level statistical testing and explainable analysis are used to characterize the resulting representations, while subject-level LOSO validation evaluates generalization to unseen participants within the available cohort. This design distinguishes the predictive utility of covariance-eigenvalue features from conventional band-power, connectivity, graph-based, and deep-learning approaches and provides a basis for future evaluation on independent EEG cohorts.

The remainder of this paper is organized as follows. Section 2 describes the materials and methods, beginning with the dataset and experimental cohort in Section 2.1 and the EEG preprocessing and covariance representation in Section 2.2. The Five-Band Covariance-Eigenvalue Representation is detailed in Section 3.1, followed by Progressive Recording-Duration Analysis and Eigenspectrum Stability assessment in Sections 3.2 and 3.3. Temporal instability, band-wise eigenvalue statistics, and

SVD-based structural dimensionality are examined in Sections 3.4–3.6. Section 3.7 describes the classifier evaluation protocol, while computational cost, SHAP-based model interpretation, feature-selection sensitivity, paired statistical validation, and the final statistical summary are presented in Sections 3.8–3.14, respectively. Section 3 overall presents the experimental results and their quantitative findings. Section 4 discusses the implications of the covariance-eigenvalue representation, its frequency- and duration-dependent behavior, and the complementary structural and interpretability analyses. Section 5 discusses the limitations of the study and directions for future work, particularly independent-cohort validation. Finally, Section 6 concludes the study by summarizing the principal findings and contributions.

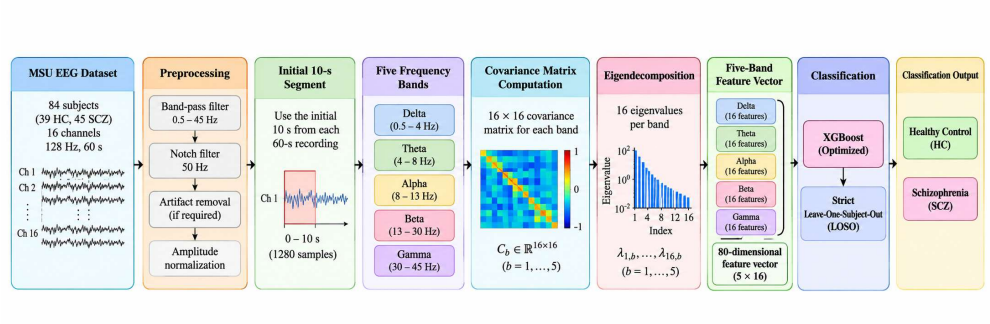


Fig. 1 Block Diagram of Proposed Method of Schizophrenia Detection

2 Materials and Methods

2.1 Dataset and Experimental Cohort

The study uses the MSU/MHRC (M. V. Lomonosov Moscow State University/Mental Health Research Center) schizophrenia EEG dataset.Dataset details and experimental configurations are presented in Table 1. The final analytical cohort consisted of 84 patients, 39 healthy controls(HC) and 45 schizophrenia(SCZ) subjects. Each recording has 16 EEG channels, sampled at 128 Hz for 60 s, leading to 7680 samples per channel in the standardized recordings.

2.2 EEG Preprocessing and Covariance Representation

Figure 2 shows an example of a raw EEG signal from the MSU dataset. Corresponding frequency responses of the applied preprocessing filters are presented in Figure 3. These include the low-pass response up to 45 Hz and the notch response at 50 Hz used to attenuate undesired frequency components.

Table 1 Dataset and Experimental Configuration

Property	Value
Subjects	84
Healthy controls	39
Schizophrenia	45
EEG channels	16
Sampling frequency	128 Hz
Recording duration	60 s
Samples/channel	7680
Primary validation	LOSO

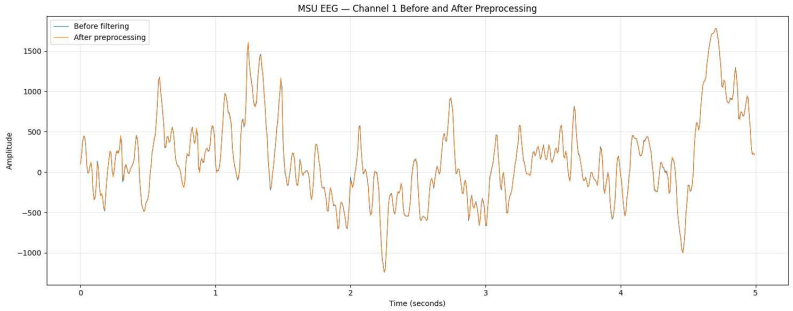


Fig. 2 EEG Signal before Preprocessing

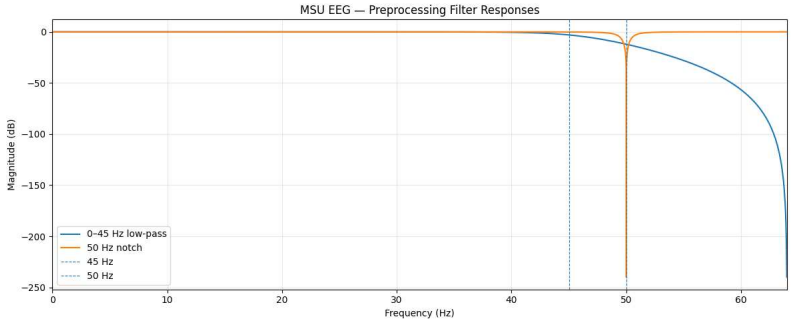


Fig. 3 EEG Signal after Preprocessing

For each subject, the multichannel EEG recording was represented as $\mathbf{X} \in \mathbb{R}^{C \times N}$, where $C = 16$ denotes the number of EEG channels and N denotes the number of temporal samples. Channel-wise mean centering was applied before covariance estimation. The covariance matrix was then constructed as

$$\mathbf{R} = \frac{\mathbf{X}\mathbf{X}^T}{N-1}. \tag{1}$$

Because $\mathbf{R}$ is symmetric positive semidefinite, its eigenvalues were obtained using symmetric eigendecomposition. The eigenvalues were sorted in descending order as

$$\lambda_1 \geq \lambda_2 \geq \cdots \geq \lambda_{16} \geq 0. \tag{2}$$

The normalized eigenspectrum was obtained by dividing each eigenvalue by the total covariance energy:

$$\tilde{\lambda}_i = \frac{\lambda_i}{\sum_{j=1}^{16} \lambda_j}, \qquad i = 1, \ldots, 16. \tag{3}$$

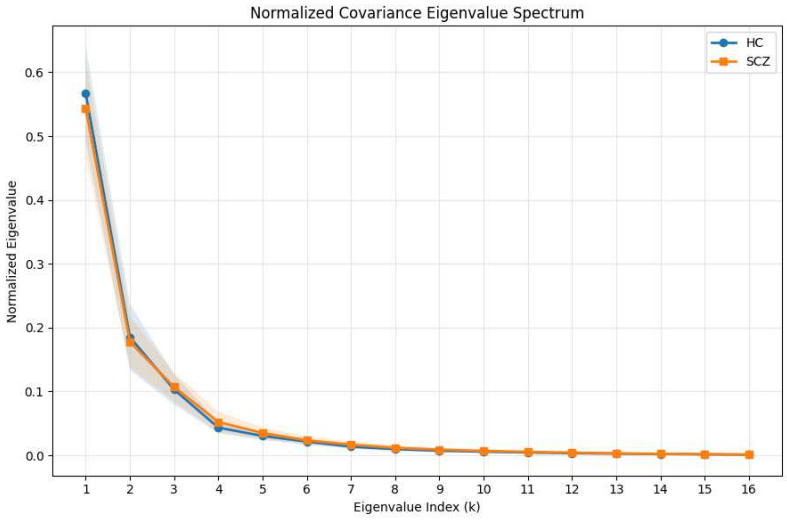


Fig. 4 Normalized Covariance Eigen Spectrum Visualization

Several compact descriptors were also derived from the covariance eigenspectrum, including total variance, maximum variance, minimum variance, leading-mode variance ratio, effective dimensionality, and spectral entropy. These descriptors were used for structural and statistical interpretation, whereas the final predictive representation used the complete five-band eigenvalue vector.

3 Results & Analysis

3.1 Five-Band Covariance-Eigenvalue Representation

TEEG was decomposed into five conventional frequency bands Delta (0.5-4 Hz), Theta (4-8 Hz), Alpha (8-13 Hz), Beta (13-30 Hz) and Gamma (30-45 Hz) in an attempt to analyze the frequency specific structure as depicted in Table 2. For each band a 16x16 covariance matrix was generated. The resulting 16 ordered eigenvalues were preserved, resulting in $16 \times 5 = 80$ features per subject.

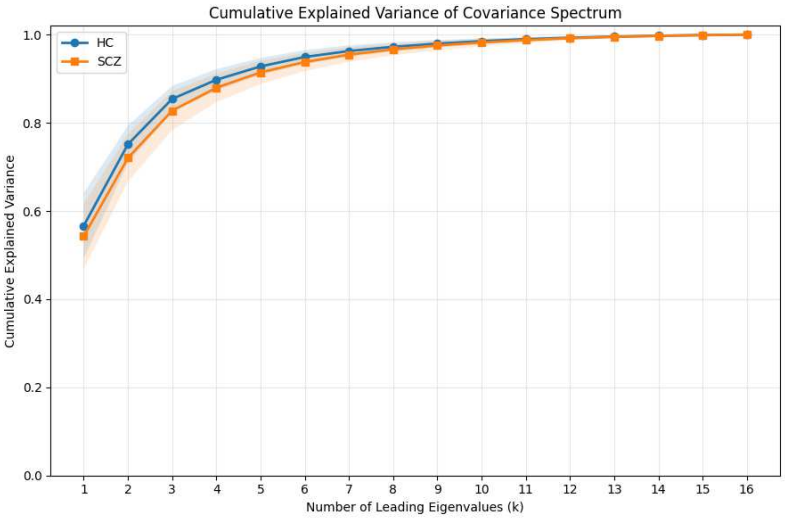


Fig. 5 Cumulative Explained Variance of Covarinace Spectrum

Table 2 Five-band covariance-eigenvalue representation.

Band	Frequency range	Eigenvalue features
Delta	0.5–4 Hz	λ_1–λ_{16}
Theta	4–8 Hz	λ_1–λ_{16}
Alpha	8–13 Hz	λ_1–λ_{16}
Beta	13–30 Hz	λ_1–λ_{16}
Gamma	30–45 Hz	λ_1–λ_{16}
Total		**80**

Table 3 Progressive-duration XGBoost screening results.

Duration (s)	Accuracy	AUC
5	0.7128	0.8171
10	0.8291	0.8974
15	0.7350	0.7903
20	0.7368	0.8239
30	0.7496	0.8199
40	0.7718	0.8268
50	0.7624	0.8399
60	0.7701	0.8598

3.2 Progressive Recording-Duration Analysis

The representation was evaluated at 5, 10, 15, 20, 30, 40, 50 and 60 s as presented in Table 3. It aimed at exploring the trade-off between recording length and classification performance and, separately, the convergence of the normalized eigenspectrum to the 60-s reference.

Table 4 Duration-dependent stability of the normalized covariance eigenspectrum.

Duration	Mean spectrum distance	Mean spectrum correlation	Mean CEV distance	Mean entropy difference	Mean D_{eff} difference
5	0.068994	0.992701	0.081484	0.105700	0.343738
10	0.050616	0.995857	0.057884	0.074860	0.253528
15	0.039501	0.997489	0.044963	0.057788	0.200154
20	0.032218	0.998370	0.036759	0.046485	0.163060
30	0.022907	0.999085	0.025649	0.032028	0.113750
40	0.016949	0.999541	0.018772	0.023680	0.084149
50	0.010678	0.999812	0.011705	0.014718	0.054500
60	0	1.000000	0	0	0

The 10-s condition yielded the best screening performance of the durations evaluated. This time was then selected for the final five-band experiment. Because the duration selection and the final assessment were done on the same cohort, the final 10-s estimate is an internally selected condition evaluation, and not an independently held-out estimate.

3.3 Eigenspectrum Stability With Recording Duration

We assessed duration-dependent stability relative to the 60-s reference using normalized spectral distance, spectral correlation, cumulative explained-variance (CEV) distance, entropy difference and effective-dimensionality difference.

Figure 4 & Table 4 shows the normalized covariance eigenspectrum for the HC and SCZ groups. The eigenvalue spectrum is focused in the first few modes, with the rest of the eigenvalues contributing progressively smaller proportions of the total covariance energy. The cumulative explained variance is presented in Figure 5 and depicts the cumulative sum of the covariance energy as additional eigenvalues are considered. The visualization provides a structural view of the covariance energy across the ordered eigenvalue modes.

Spectral similarity increased monotonically with duration. The mean spectral correlation to the 60-s reference was 0.995857 and the mean spectral distance was 0.050616 at 10 s. It reveals that structural stability and classification discriminability are related but separate properties: increasing stability did not lead to a monotonic improvement in classification performance.

3.4 Temporal-Instability Analysis

Temporal variability was evaluated by comparing segment-level eigenspectral descriptors between healthy controls and schizophrenia subjects. Five frequency bands were evaluated by group-wise statistical analyzes, then corrected for false-discovery rate (FDR).

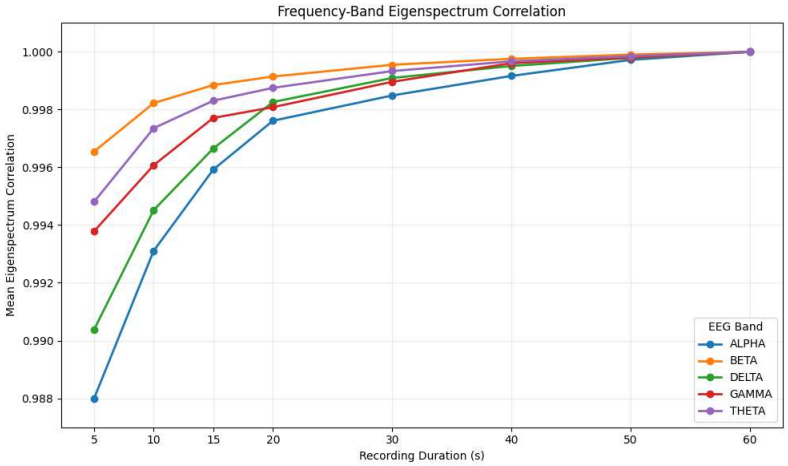


Fig. 6 Frequency Band Eigen Spectrum Correlation

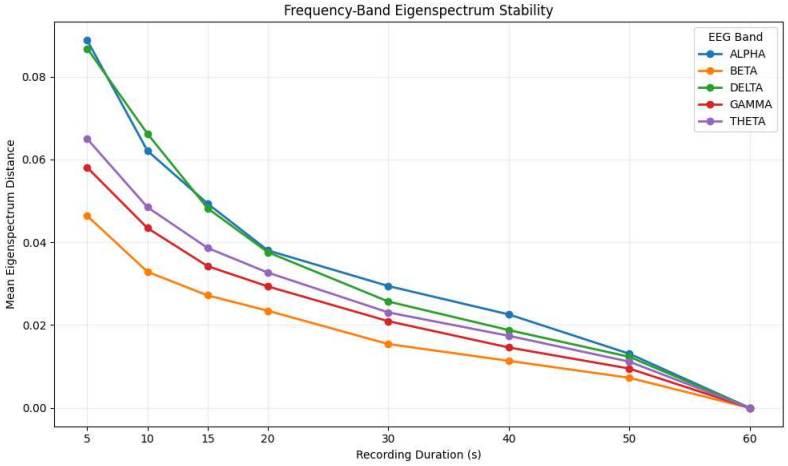


Fig. 7 Frequency Band Eigen Spectrum Stability

Table 5 Group differences in temporal-instability measures.

Band	**HC mean ± SD**	**SCZ mean ± SD**	**Raw p**	**FDR p**	**Rank-biserial r**
Delta	-0.0169 ± 0.8520	0.0147 ± 0.8727	0.60292	0.60292	-0.0667
Theta	-0.2674 ± 0.7912	0.2317 ± 0.7782	0.00543	0.02715	-0.3539
Alpha	-0.1427 ± 0.8347	0.1237 ± 0.7750	0.14874	0.24790	-0.1841
Beta	-0.2402 ± 0.5321	0.2082 ± 0.9371	0.01114	0.02785	-0.3231
Gamma	-0.1011 ± 0.8564	0.0876 ± 0.7421	0.24727	0.30909	-0.1476

Table 5 presents the group-wise comparison of temporal-instability measures across the five EEG frequency bands. The results indicate frequency-specific differences

Table 6 Bootstrap effect estimates for significant temporal-instability differences.

Band	Mean difference	Bootstrap 95% CI	Cohen's d
Theta	0.4991	0.1683–0.8304	0.6364
Beta	0.4483	0.1464–0.7893	0.5776

between the HC and SCZ groups. Although the raw p-values indicated significant differences in the theta ($p = 0.00543$) and beta ($p = 0.01114$) bands, only these two differences remained statistically significant after FDR correction, with adjusted p-values of 0.02715 and 0.02785, respectively. The corresponding rank-biserial correlations were -0.3539 for theta and -0.3231 for beta, indicating moderate group-level differences. In contrast, the delta, alpha, and gamma bands did not remain significant after FDR correction, suggesting that their observed differences were not sufficiently robust under multiple-comparison control.

Table 6 presents the bootstrap effect estimates for the significant theta- and beta-band differences. The theta band showed a mean group difference of 0.4991 with a 95% bootstrap confidence interval of 0.1683–0.8304 and Cohen's $d = 0.6364$, whereas the beta band showed a mean difference of 0.4483 with a 95% confidence interval of 0.1464–0.7893 and Cohen's $d = 0.5776$. The confidence intervals exclude zero for both frequency bands, supporting the robustness of the observed group differences, while the Cohen's d values indicate moderate effect sizes. These findings suggest that theta- and beta-band temporal-instability measures capture meaningful differences in EEG dynamics between HC and SCZ subjects, providing an important temporal-domain observation that complements the subsequent covariance-eigenvalue analysis.

A separate, segment-wise trajectory analysis included 275 comparisons. Of the 31 comparisons with raw $p < 0.05$, none survived after FDR correction; the minimum FDR-adjusted p-value was 0.103614. Thus, the corrected evidence is limited to the composite Theta and Beta temporal-instability measures rather than to individual segment-wise trajectories.

Figure 7 depicts the stability of the normalized covariance eigenspectrum of the five EEG frequency bands as a function of duration. As the recording duration increases, the mean eigenspectrum distance drops gradually for all frequency bands, and reaches zero at 60 s. At shorter durations, the magnitude of the distance varies between frequency bands, but the spectra converge to the 60-s reference with increasing recording duration. The analysis provides a frequency-specific view on the convergence of the eigenspectrum of covariance with the recording duration.

The correlation of the frequency-band eigenspectrum for the measured recording periods with the 60-s reference is shown in Figure 6. All five frequency bands show an increase in the correlation with recording duration demonstrating an increasing similarity between the duration-specific eigenspectra and the 60s reference spectrum. At 60 s, the correlation is 1.000 for all bands by definition of the reference condition.

Table 7 FDR-significant band-wise eigenvalue comparison.

Feature	HC mean	SCZ mean	Raw p	FDR p	Effect size d
Alpha λ_1	668424.51	362436.18	0.000052	0.004186	−0.686445

Results demonstrate the rapid convergence of the normalized eigenspectrum across frequency bands for increasing recording duration.

3.5 Band-Wise Eigenvalue Statistical Analysis

The five-band model produced 80 eigenvalue comparisons (5 bands × 16 ordered eigenvalues). Seven comparisons exhibited raw p-values below 0.05, with only one remaining statistically significant after false discovery rate (FDR) correction. The sole FDR-significant comparison was the first eigenvalue of the alpha-band covariance matrix ($\alpha\lambda_1$), indicating that the dominant covariance component within the alpha band exhibited a significant group-level difference between HC and SCZ subjects.

Table 7 presents the FDR-significant band-wise eigenvalue comparison. The mean value of $\alpha\lambda_1$ was substantially higher in the HC group (668424.51) than in the SCZ group (362436.18), with a raw p-value of 0.000052 and an FDR-adjusted p-value of 0.004186. The corresponding effect size was large ($d = -0.686445$), indicating a substantial difference in the dominant alpha-band covariance component between the two groups. This finding provides direct statistical evidence that the covariance-eigenvalue spectrum captures frequency-specific alterations associated with schizophrenia. Importantly, the result also demonstrates that the discriminative information is not uniformly distributed across all eigenvalues and frequency bands, motivating the subsequent structural analysis of the covariance spectrum using SVD.

The leading eigenvalue of the alpha-band showed a moderate to large standardized group difference. Additional effect-size evaluation revealed alpha λ_1 with $d = -0.686$ (95% CI −1.159 to −0.284) and R80 with $d = 0.588$ (95% CI 0.192 to 1.029). These findings are interpreted as statistical properties of covariance structure rather than evidence for a specific neural generator.

3.6 SVD-Based Structural Dimensionality

Singular value decomposition presents the equivalent mathematical interpretation of covariance energy, given that the eigenvalues of covariance are related with the squared singular values of the centered data matrix. Thus, SVD was utilized as a structural interpretation to determine the quantity of orthogonal modes needed to explain particular variance proportions.

As summarized in Table 8, the SCZ group exhibited higher structural dimensionality than the HC group across the $R80$, $R90$, and $R95$ measures. Specifically, the mean number of modes required to explain 80%, 90%, and 95% of the covariance energy increased from 2.9744, 4.5128, and 6.5128 in HC subjects to 3.2444, 4.9556, and 7.0667 in SCZ subjects, respectively. All three measures remained significant after FDR correction ($p_{\mathrm{FDR}} = 0.03848$). The energy entropy and energy effective rank also showed higher mean values in SCZ (1.5153 and 4.6149, respectively) than

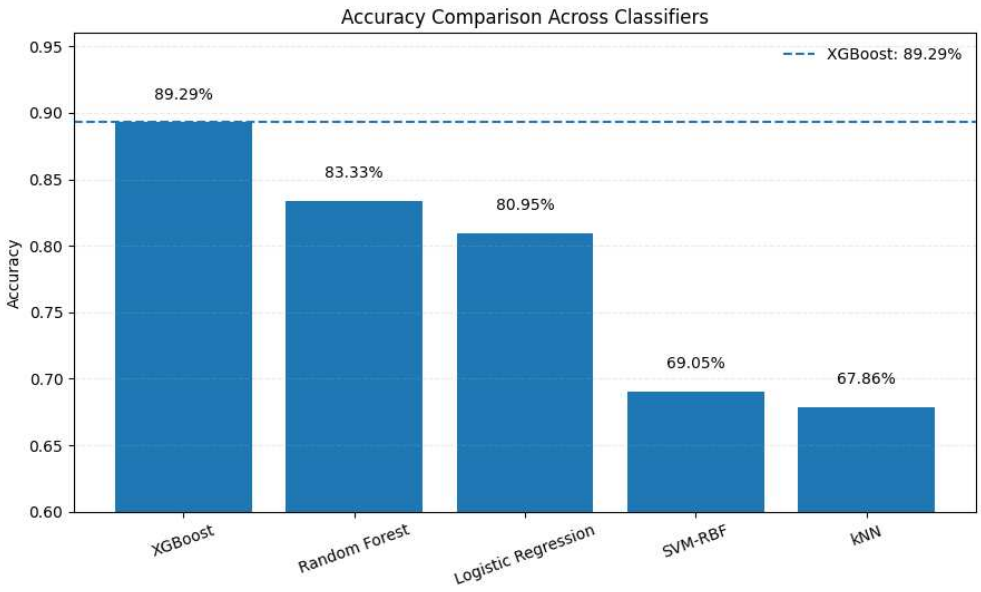


Fig. 8 Accuracy Comparison among the Evaluated Classifiers.

Table 8 SVD-derived structural dimensionality and energy-distribution measures.

Measure	**HC mean**	**SCZ mean**	**FDR p**
R80	2.9744	3.2444	0.03848
R90	4.5128	4.9556	0.03848
R95	6.5128	7.0667	0.03848
Energy entropy	1.4276	1.5153	0.03848
Energy effective rank	4.2126	4.6149	0.03848
SV entropy	—	—	0.05108
SV effective rank	—	—	0.05108

in HC (1.4276 and 4.2126), with both comparisons remaining significant after FDR correction ($p_{\mathrm{FDR}} = 0.03848$). These findings indicate that the SCZ covariance spectra require a greater number of orthogonal modes to account for the same proportion of covariance energy and exhibit a more distributed energy structure. In contrast, the singular-value entropy and singular-value effective-rank measures did not reach the FDR significance threshold ($p_{\mathrm{FDR}} = 0.05108$). Therefore, the SVD results provide a complementary structural interpretation of the covariance spectrum, suggesting increased dimensionality and energy dispersion in SCZ without introducing these measures as an independent predictive feature category.

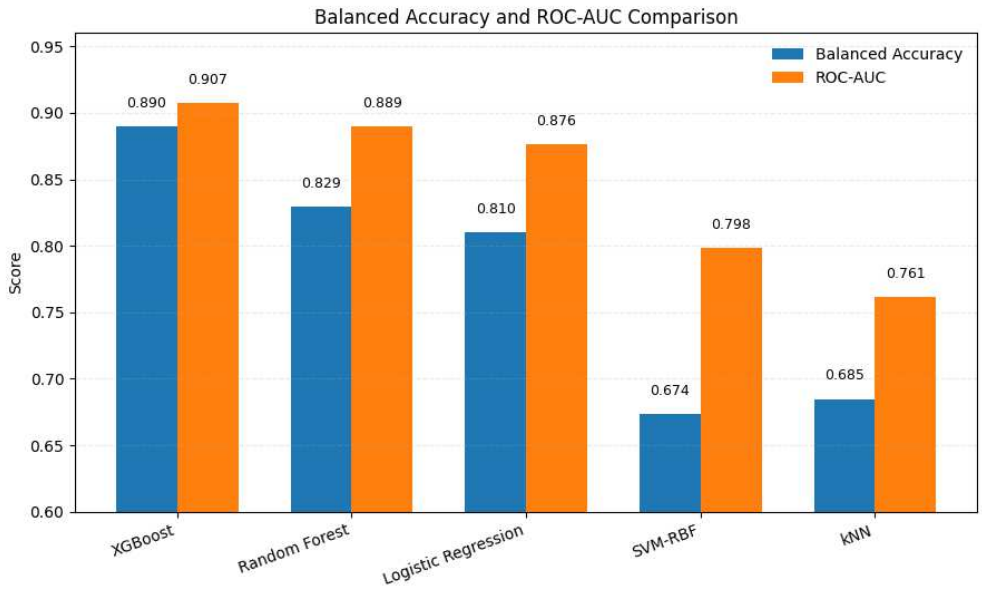


Fig. 9 Accuracy-ROC Comparison among the Evaluated Classifiers.

3.7 Classifier Evaluation

The final 10-second five-band covariance-eigenvalue representation contained 80 numerical features for each participant. Five classification algorithms were assessed on the same 84 participants using rigorous Leave-One-Subject-Out (LOSO) methodology: XGBoost, Random Forest, Logistic Regression, Support Vector Machine with a Radial Basis Function kernel, and k-nearest neighbors. XGBoost used 200 estimators, a maximum depth of 3, a learning rate of 0.05, a subsample ratio of 0.8, column subsampling of 0.8, and a random state of 42. Figure 8 Figure 11, Figure 9 shows the Accuracy, ROC-AUC, and Balanced Accuracy performance comparison of the different classifiers considered in this experimental study.

Table 9 provides the complete subject-level performance under the same strict LOSO protocol. XGBoost achieved the highest overall performance, with an accuracy of 0.8929, balanced accuracy of 0.8897, ROC-AUC of 0.9071, sensitivity of 0.9333, and specificity of 0.8462. Random Forest provided the second-best overall performance, with an accuracy of 0.8333 and ROC-AUC of 0.8895. Logistic Regression achieved an accuracy of 0.8095 and ROC-AUC of 0.8764, whereas SVM-RBF and kNN yielded lower accuracies of 0.6905 and 0.6786, respectively. The corresponding confusion-matrix components further show that XGBoost correctly identified 12 SCZ subjects and 33 HC subjects, with 3 false negatives and 6 false positives. The consistently stronger performance of XGBoost across accuracy, balanced accuracy, sensitivity, and ROC-AUC indicates that the proposed 80-dimensional covariance-eigenvalue representation can support effective subject-level discrimination when combined with a nonlinear ensemble classifier. Importantly, these results were obtained without subject

Table 9 Same-test classifier comparison under strict LOSO.

Classifier	Acc.	BA	AUC	Sens.	Spec.	TN	FP	FN	TP
XGBoost	0.8929	0.8897	0.9071	0.9333	0.8462	33	6	3	42
Random Forest	0.8333	0.8291	0.8895	0.8889	0.7692	30	9	5	40
Logistic Regression	0.8095	0.8103	0.8764	0.8000	0.8205	32	7	9	36
SVM-RBF	0.6905	0.6735	0.7983	0.9111	0.4359	17	22	4	41
kNN	0.6786	0.6846	0.7613	0.6000	0.7692	30	9	18	27

Table 10 Measured computational time for the five classifiers.

Classifier	Total time (s)	Mean LOSO-fold time (s)
SVM-RBF	0.6315	0.0075
Logistic Regression	2.8956	0.0345
kNN	0.4234	0.0050
Random Forest	106.9171	1.2728
XGBoost	14.3564	0.1709

overlap between training and testing folds, ensuring that the reported performance reflects subject-level generalization rather than segment-level classification.

3.8 Computational Cost

The timing measurements reflect the recorded execution environment and should be interpreted as implementation-specific rather than hardware-independent complexity measures. Table 10 summarizes the total execution time and mean LOSO-fold execution time for the five classifiers. SVM-RBF required the lowest total computational time (0.6315 s), followed by kNN (0.4234 s) and Logistic Regression (2.8956 s), while Random Forest required the highest total time (106.9171 s). XGBoost required 14.3564 s in total, corresponding to a mean LOSO-fold time of 0.1709 s. Although XGBoost was not the fastest classifier, its computational requirement remained substantially lower than that of Random Forest while providing the strongest predictive performance across the evaluated measures. The timing results therefore illustrate a practical trade-off between computational cost and predictive performance, with XGBoost providing a favorable balance for the final experimental configuration.

3.9 SHAP-Based Model Interpretation

To investigate the contribution of the covariance-eigenvalue representation to the final XGBoost model, a global SHAP analysis was performed on the complete 80-feature representation. The analysis ranks features according to their mean absolute SHAP values, thereby identifying the features that contribute most strongly to the model predictions. The top 20 features are presented in Table 12. The ranked features span all five EEG frequency bands, indicating that the predictive information is distributed across the frequency-specific covariance structure rather than being confined to a single band. Several of the highest-ranked features are associated with the alpha and

Table 11 Subject-level bootstrap 95% confidence intervals; 10,000 valid resamples per classifier.

Classifier	Accuracy (95% CI)	Balanced Accuracy (95% CI)	Sensitivity (95% CI)	Specificity (95% CI)	ROC-AUC (95% CI)
XGBoost	0.8929 (0.8214–0.9524)	0.8897 (0.8176–0.9524)	0.9333 (0.8500–1.0000)	0.8462 (0.7234–0.9500)	0.9071 (0.8315–0.9685)
Random Forest	0.8333 (0.7500–0.9048)	0.8291 (0.7440–0.9060)	0.8889 (0.7872–0.9762)	0.7692 (0.6316–0.8947)	0.8895 (0.8062–0.9575)
Logistic Regression	0.8095 (0.7262–0.8929)	0.8103 (0.7225–0.8929)	0.8000 (0.6750–0.9091)	0.8205 (0.6905–0.9310)	0.8764 (0.7912–0.9459)
SVM-RBF	0.6905 (0.5833–0.7857)	0.6735 (0.5857–0.7614)	0.9111 (0.8182–0.9796)	0.4359 (0.2821–0.5897)	0.7983 (0.6960–0.8861)
kNN	0.6786 (0.5833–0.7738)	0.6846 (0.5856–0.7784)	0.6000 (0.4565–0.7391)	0.7692 (0.6279–0.8947)	0.7613 (0.6558–0.8547)

Table 12 Top 20 global SHAP features for descriptive interpretation.

Rank	Feature	Mean Absolute SHAP	Band	Eigenvalue Rank
1	alpha_lambda_1	0.948121	Alpha	1
2	alpha_lambda_16	0.593186	Alpha	16
3	gamma_lambda_15	0.385068	Gamma	15
4	gamma_lambda_14	0.359688	Gamma	14
5	alpha_lambda_2	0.321911	Alpha	2
6	gamma_lambda_16	0.320073	Gamma	16
7	theta_lambda_7	0.315744	Theta	7
8	beta_lambda_1	0.268769	Beta	1
9	delta_lambda_15	0.231728	Delta	15
10	beta_lambda_16	0.216129	Beta	16
11	delta_lambda_2	0.199213	Delta	2
12	delta_lambda_12	0.163832	Delta	12
13	delta_lambda_16	0.163170	Delta	16
14	alpha_lambda_3	0.125307	Alpha	3
15	delta_lambda_8	0.117851	Delta	8
16	gamma_lambda_13	0.099767	Gamma	13
17	beta_lambda_14	0.078404	Beta	14
18	alpha_lambda_4	0.075163	Alpha	4
19	delta_lambda_1	0.071637	Delta	1
20	delta_lambda_14	0.066146	Delta	14

gamma bands, including alpha_λ_1, alpha_λ_{16}, and gamma_λ_{15}. The presence of different eigenvalue ranks among the highly ranked features further suggests that both dominant and lower-variance components of the covariance structure contribute to the classification decision. Thus, the SHAP analysis provides an interpretable view of how the frequency-specific eigenvalue representation contributes to schizophrenia discrimination.

3.10 Feature-Selection Sensitivity Analysis

The stability of the selected feature representation was further examined using nested SHAP/ANOVA feature-selection and local-neighborhood sensitivity analyses.

As shown in Table 14, SHAP was selected in 58 of the 84 outer folds (69.05%), compared with 26 folds (30.95%) for ANOVA, indicating a higher frequency of selection for the model-based attribution approach. The distribution of the selected neighborhood parameter K in the nested analysis is summarized in Table 15. The selected values were distributed across the tested range, with $K = 60$ occurring most frequently (26.19%). These results indicate that the feature-selection procedure did not converge exclusively to a single small neighborhood size.

The effect of feature reduction was then compared against the complete 80-feature representation. As reported in Table 16, nested SHAP/ANOVA selection reduced accuracy, balanced accuracy, and sensitivity relative to the complete representation, although ROC-AUC increased from 0.9071 to 0.9151. Similarly, the local-K refinement in Table 17 resulted in reductions in accuracy, balanced accuracy, sensitivity, and ROC-AUC, while specificity increased from 0.8462 to 0.8718. Therefore, neither feature-selection strategy provided a consistent improvement across the evaluation measures. Based on this sensitivity analysis, the complete 80-feature representation was retained for the final experiment, preserving the information contained in the frequency-specific covariance-eigenvalue structure rather than applying an additional feature-reduction step.

3.11 Final Statistical Validation and Robustness Analysis

The reliability of the final 80-feature representation was assessed through subject-level bootstrap resampling and paired statistical comparisons between classifiers. Table 11 presents the performance estimates and 95% confidence intervals obtained from 10,000 valid subject-level bootstrap resamples. The XGBoost model achieved an accuracy of 0.8929, balanced accuracy of 0.8897, sensitivity of 0.9333, specificity of 0.8462, and ROC-AUC of 0.9071. The bootstrap analysis provides an estimate of the variability of these measures at the subject level and complements the single-point performance estimates obtained from the LOSO evaluation.

To determine whether the observed differences between XGBoost and the comparator classifiers were statistically meaningful, exact McNemar tests were performed on the paired subject-level predictions, followed by Holm correction for multiple comparisons. As shown in Table 13, the comparisons between XGBoost and SVM-RBF and between XGBoost and kNN remained statistically significant after correction, with Holm-adjusted p-values of 0.004541 and 0.001109, respectively. In contrast, the comparisons with Random Forest and Logistic Regression were not statistically significant after Holm correction. These results indicate that the predictive advantage of XGBoost is particularly evident relative to SVM-RBF and kNN, while the differences from Random Forest and Logistic Regression should not be interpreted as statistically significant. Together, the bootstrap and paired statistical analyses provide complementary evidence regarding the robustness and statistical reliability of the final model.

SHAP analysis was conducted on the final XGBoost model applied to all 84 subjects for the purpose of descriptive model interpretation. This analysis was not utilized as an independent performance assessment. The SHAP matrix comprised 84 subjects and 80 features.

Table 13 Exact McNemar tests with Holm correction.

Comparison	XGB–C	XGB–W	Discordant	Exact p	Holm p	Sig.
XGB vs RF	7	2	9	0.179688	0.334137	No
XGB vs LR	13	6	19	0.167068	0.334137	No
XGB vs SVM-RBF	22	5	27	0.001514	0.004541	Yes
XGB vs KNN	21	3	24	0.000277	0.001109	Yes

XGB–C: XGB correct and comparator wrong; XGB–W: XGB wrong and comparator correct; Sig.: significant after Holm correction.

Table 14 Method selection frequency in nested feature-selection analysis.

Method	Outer-fold selections
SHAP	58/84 (69.05%)
ANOVA	26/84 (30.95%)

3.12 Feature-Selection Sensitivity Analysis

Nested SHAP and ANOVA methodologies for feature selection were examined as a sensitivity analysis. The outer test subject was excluded from feature ranking and local K selection; rankings were calculated within inner training folds, and the final model was fitted only on the outer training data. Among the 84 outer folds, SHAP was chosen in 58 folds while ANOVA was utilized in 26 folds. The originally selected K values spanned from 10 to 80, with $K = 60$ emerging as the most frequent choice (22 out of 84 folds.

The SHAP analysis enhances the interpretability of the proposed model by pinpointing the most significant covariance–eigenvalue features that influence the XGBoost predictions. The top 20 features are mainly associated with the alpha, gamma, theta, beta, and delta frequency bands, with alpha $-\lambda_1$, alpha $-\lambda_{16}$, and gamma $-\lambda_{15}$ demonstrating very significant effects on the model's results. The distribution of SHAP values reveals that these eigenvalue-based features influence the classification decision differently based on their magnitude, demonstrating that the model captures discriminative frequency-specific EEG characteristics instead of depending on a single feature. This feature-level explanation offers additional evidence for the relevance of the proposed covariance–eigenvalue representation in differentiating healthy controls from those with schizophrenia. Figure 10 shows the SHAP experiment summary.

The nested SHAP/ANOVA methodology produced an outer-LOSO performance of 88.10% accuracy, 87.86% balanced accuracy, 91.51% ROC-AUC, 91.11% sensitivity, and 84.62% specificity. In comparison with the comprehensive 80-feature representation, both accuracy and balanced accuracy diminished, although ROC-AUC experienced a slight gain.

A further local refinement of $K = 55$–65 was executed utilizing the method inherited from the nested analysis. The chosen K values were evenly spread throughout

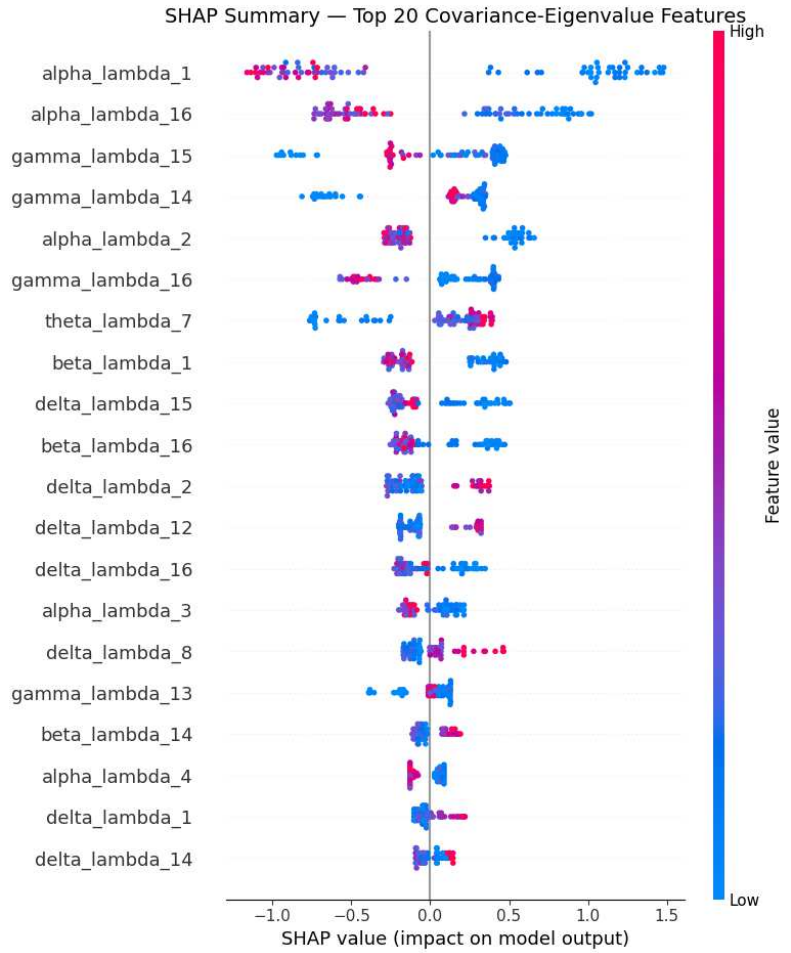


Fig. 10 Shap Analysis

Table 15 Selected K frequency in the original nested SHAP/ANOVA experiment.

K	**Number of folds**	**Percentage**
10	5	5.95%
15	5	5.95%
20	9	10.71%
30	15	17.86%
40	17	20.24%
60	22	26.19%
80	11	13.10%

the full local range, yielding an outer performance of 85.71% accuracy, 85.81% balanced accuracy, 90.43% ROC-AUC, 84.44% sensitivity, and 87.18% specificity. This

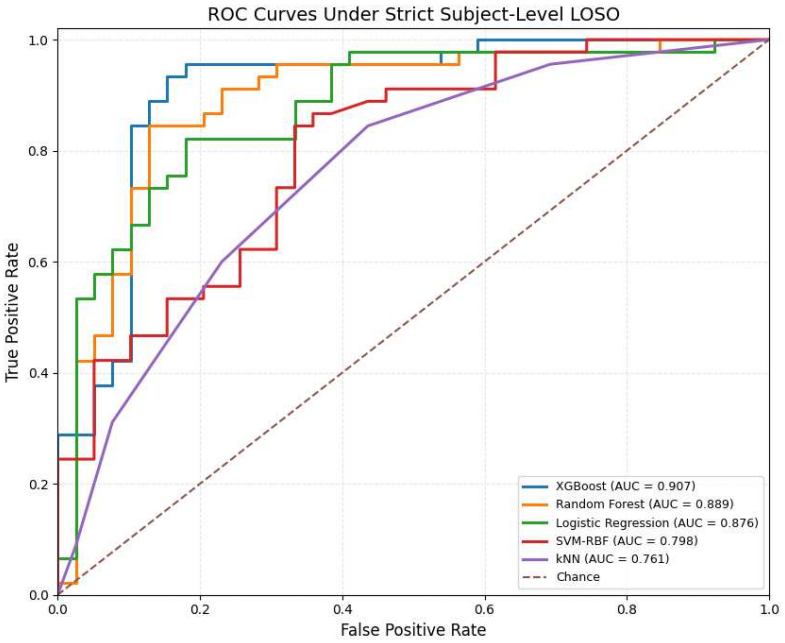


Fig. 11 ROC AUC Curve

Table 16 Complete representation versus nested SHAP/ANOVA feature selection.

Metric	80-feature XGBoost	Nested SHAP/ANOVA	Difference
Accuracy	0.8929	0.8810	−0.0119
Balanced Accuracy	0.8897	0.8786	−0.0111
Sensitivity	0.9333	0.9111	−0.0222
Specificity	0.8462	0.8462	≈ 0
ROC-AUC	0.9071	0.9151	+0.0080

Table 17 Local K refinement versus the locked 80-feature representation.

Metric	80-feature XGBoost	Local $K = 55$–65	Difference
Accuracy	0.8929	0.8571	−0.0358
Balanced Accuracy	0.8897	0.8581	−0.0316
ROC-AUC	0.9071	0.9043	−0.0028
Sensitivity	0.9333	0.8444	−0.0889
Specificity	0.8462	0.8718	+0.0256

enhancement failed to augment the overall depiction and was thus not adopted as the final predictive model.

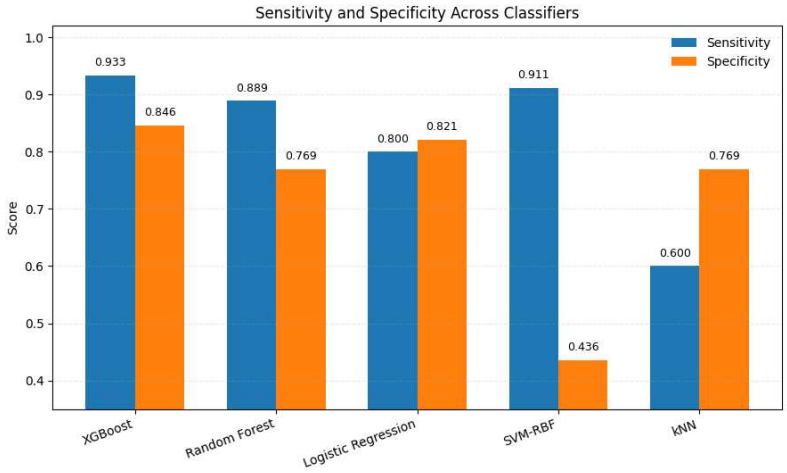


Fig. 12 Sensitivity Vs Specificity

These sensitivity analyses support retention of the complete 80-dimensional covariance-eigenvalue representation. SHAP is consequently treated as an interpretability tool rather than a feature-selection mechanism. Figure 12 shows sensitivity and specificity performance of classifiers took part in this study.

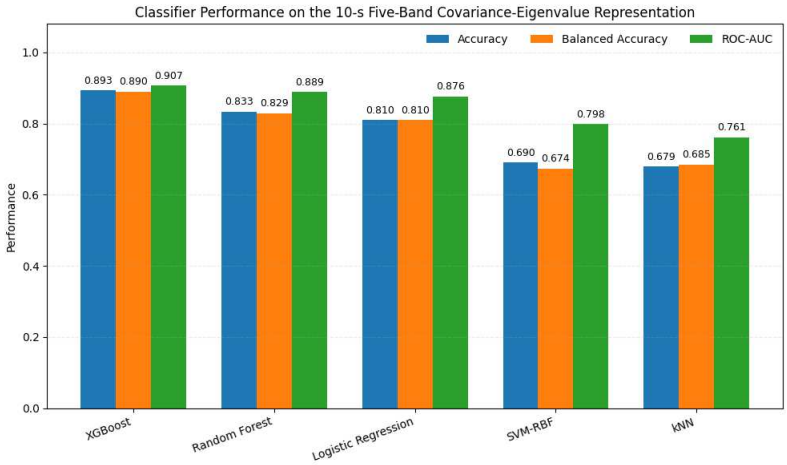


Fig. 13 Performance Comparison of Various Classifiers

3.13 Paired Statistical Validation of Classifiers

Since all classifiers produced predictions for the same 84 subjects, paired exact McNemar tests were utilized to analyze their prediction-error patterns. Four comparisons

were carried out against XGBoost: Random Forest, Logistic Regression, SVM-RBF, and kNN. The Holm correction was applied across the four paired comparisons.

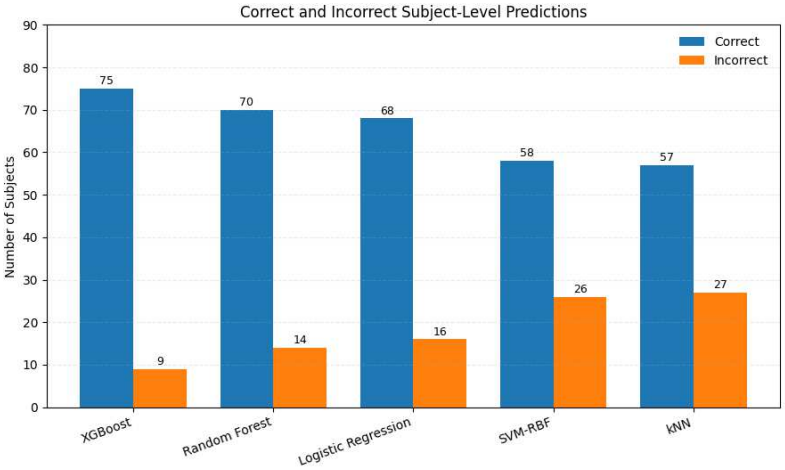


Fig. 14 Correct and Incorrect Prediction Analysis

The paired error patterns exhibited notable differences between XGBoost and SVM-RBF, as well as between XGBoost and kNN after Holm correction. The comparisons against Random Forest and Logistic Regression were not statistically significant after correction. These tests compare paired prediction-error patterns; they do not establish universal superiority of a single classifier.

3.14 Final Statistical Summary

Figure 13 and Figure 14 present a comparative analysis of the classifiers utilizing proposed five-band covariance-eigenvalue framework. As illustrated in Figure 13, XGBoost has excellent overall performance, attaining an accuracy of 89.3%, a balanced accuracy of 89.0%, and a ROC-AUC of 90.7%, surpassing Random Forest, Logistic Regression, SVM-RBF, and KNN. In alignment with these findings, Figure 14 illustrates that XGBoost accurately categorizes 75 out of 84 subjects, yielding merely 9 incorrect predictions, so showcasing its exceptional subject-level classification competence.

The findings give converging evidence from predictive, statistical and structural analyzes. The five-band covariance–eigenvalue representation produced a compact 80-dimensional representation, preserving group-related information under subject-level LOSO evaluation. Among the classifiers examined, the XGBoost classifier yielded the best observed accuracy, balanced accuracy, and ROC-AUC in the same-test comparison. Figure 15 shows confusion matrix of 84 subjects consisted of 33 true negatives, 6 false positives, 3 false negatives and 42 true positives.

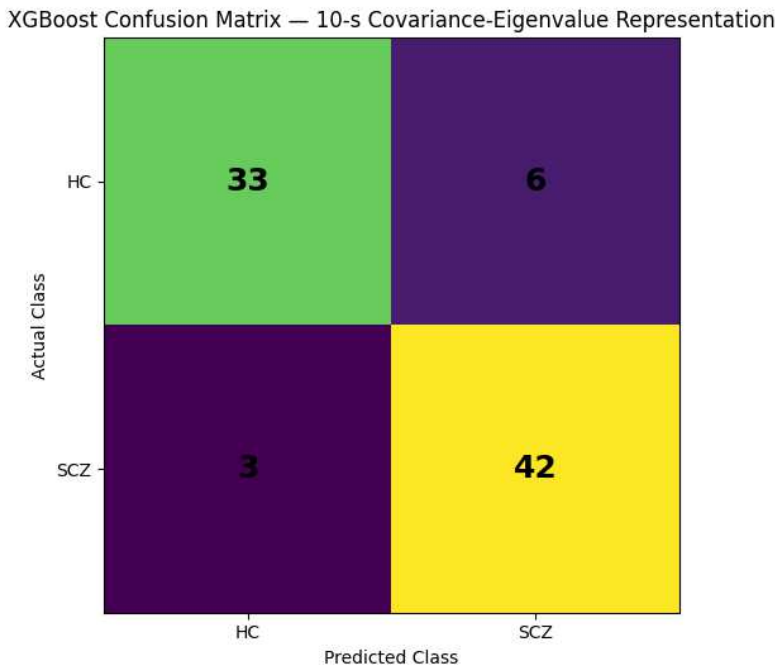


Fig. 15 Confusion Matrix XGBoost

The bootstrap analysis revealed that the point estimates are accompanied by a non-negligible uncertainty as expected for a cohort of 84 subjects. XGBoost had a 95% bootstrap interval of 0.8214–0.9524 for accuracy, 0.8176–0.9524 for balanced accuracy, 0.8500–1.0000 for sensitivity, 0.7234–0.9500 for specificity, and 0.8315–0.9685 for ROC-AUC.

Figure 16 shows the subject-level bootstrap performance estimates with 95% confidence intervals for the five classifiers. The XGBoost estimates indicate a relatively high accuracy, balanced accuracy, sensitivity, specificity, and ROC-AUC with the corresponding confidence intervals capturing the level of uncertainty due to the 84-subject cohort. The other classifiers exhibit varying degrees of performance and uncertainty across the evaluated metrics. These bootstrap intervals complement the point estimates by illustrating the variability of the performance measures under subject-level resampling.

The paired classifier analysis found 22 cases where XGBoost was accurate and SVM-RBF was wrong and 5 situations where in the reverse direction, with a Holm-adjusted p-value of 0.004541. For XGBoost versus kNN the respective discordant counts were 21 and 3 with Holm-adjusted $p = 0.001109$. Differences versus Random Forest and Logistic Regression did not survive Holm correction.

The duration study demonstrated a difference between representation stability and predictive discrimination. The normalized eigenspectrum became more similar to the 60-s reference as duration increased, but the classification accuracy did not rise monotonically. The 10-s condition, which performed best in the screening experiment, was

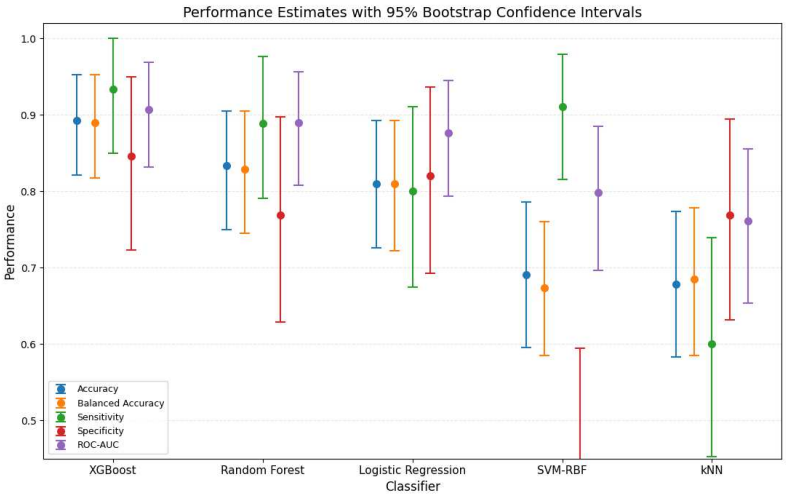


Fig. 16 Bootstrap Results

Table 18 Comparison of existing schizophrenia detection methods with the proposed work.

Study	Features	Method	Dataset	Validation	Acc. (%)
Grace Neethu P et al. [2026]	VMD-based VIMF features	VMD + ANOVA + RF	MSU	NR	82.35
Xinran Han et al. [2026]	Multiscale hand-crafted EEG features + mRMR	Ensemble Learning + mRMR	MSU	LOSO	77.38
GS Sravanthi et al. [2026]	Multi-domain (time, frequency, nonlinear)	VMD + Optimized ML	MSU	LOOCV	81.55
Proposed Work	**Five-band covariance eigenvalues (80 features)**	**XGBoost**	**MSU**	**LOSO**	**89.29**

therefore chosen for the final analysis. This selection is cohort-internal and should not be interpreted as an independent validation of a universal 10-s recording requirement.

The temporal analysis showed significant FDR-corrected group differences in Theta and Beta instability. The 275-comparison segment-wise trajectory analysis did not return any FDR-significant individual comparison. Band-wise eigenvalue analysis revealed that only Alpha λ_1 eigenvalue comparison survived FDR correction. SVD-derived cumulative energy ranks and energy-based entropy/effective rank were likewise higher in SCZ after correction.

4 Discussion

This work's main contribution is the systematic study of covariance eigenvalue spectrum as an interpretable second-order representation of multichannel EEG. Instead of using the raw EEG samples or a wide set of heterogeneous descriptors, the framework summarizes the distribution of covariance energy over orthogonal modes in channel

space . Then the same representation can be investigated from the complementary perspective of frequency, temporal, duration and dimensionality.

Table 18 provides a contextual comparison of the proposed approach with existing schizophrenia detection methods evaluated on the MSU EEG dataset. Unlike approaches that primarily rely on handcrafted time- or frequency-domain descriptors, the proposed framework characterizes the underlying multichannel EEG structure through the eigenvalue spectrum of frequency-specific covariance matrices. The eigenvalues provide a compact representation of the distribution of variance and inter-channel dependency within each frequency band, thereby reducing the high-dimensional covariance structure to a set of interpretable spectral descriptors. In the proposed configuration, the five frequency bands generate 80 eigenvalue-based features, which are subsequently used by XGBoost for classification. Importantly, the evaluation follows a strict subject-level leave-one-subject-out (LOSO) strategy, ensuring that recordings from the same subject do not appear in both training and testing sets. Although accuracy is reported in Table 18 to facilitate comparison with previous studies, the primary significance of the proposed framework lies in demonstrating the discriminative and interpretable information contained in the frequency-specific covariance eigenvalue structure, rather than in accuracy alone. The obtained 89.29% accuracy further indicates that this compact structural representation retains sufficient information for effective subject-level schizophrenia discrimination.

The results of the five bands show that the information is not limited to one frequency range. The single band analysis demonstrated the best observed performance for Gamma, with contributions from Delta and Theta to the fused representation. Temporal-instability analysis results provide a complementary observation .Theta and Beta showed corrected group differences in temporal variability . Together, these results indicate that the covariance-eigenvalue representation contains frequency-dependent and temporally varying group-related information.

The duration findings are particularly important for interpretation. The stability of the eigenspectrum is improved by adding more data but the classification performance does not change in a monotonic way with duration. Thus, stability and discriminability should not be treated as interchangeable properties. The high 10-s spectral correlation with the 60-s reference indicates rapid structural convergence, but the separate classification study demonstrates that the most stable representation is not automatically the most discriminative.

The classifier comparison favors the adoption of XGBoost for final fixed representation in this cohort. The McNemar analysis offers more detail than point estimates alone. The paired error pattern of XGBoost was statistically different from SVM-RBF and kNN, but not significantly different from Random Forest and Logistic Regression after Holm correction. Thus, the results should be seen not as evidence that XGBoost is universally superior, but rather as a record of observed performance and paired-error relationships under the experimental technique used.

SHAP analysis revealed that `alpha_lambda_1` is the most crucial global feature followed by `alpha_lambda_16` and several Gamma and Alpha eigenvalues. However, feature prominence does not imply causality. The nested feature-selection tests also

revealed that selecting subsets of eigenvalues did not improve upon the complete representation. Thus, the full covariance-eigenvalue structure is preserved by retaining all 80 features, without introducing a model-dependent feature-selection layer for which a predictive benefit has not been demonstrated.

The SVD analysis gives a complementary mathematical interpretation. Higher cumulative-energy rankings and energy effective rank in SCZ imply more covariance/SVD modes are needed to capture specified fractions of variance in the group comparison. Mathematically, covariance eigenvalues and squared singular values are linked, SVD is treated as an interpretive reformulation rather than an independent source of predictive evidence.

5 Limitations and Future Work

First, the study uses a single cohort of 84 subjects from one acquisition environment, limiting statistical power and generalizability. Second, the last 10-s operating point was selected based on duration screening on the same cohort. Although subject-level LOSO protects each individual prediction from direct subject leakage, but the process of duration selection means that there is a selection component which is not comparable to an independently held-out duration evaluation. The final estimate of 89.29

Third, covariance eigenvalues and SVD-derived rankings are mathematical descriptors of multichannel variance organization. Without independent neurophysiological data they should not be considered as direct assessments of neuronal generators, anatomical pathways or connection mechanisms. Fourth, preprocessing, electrode montage, choice of reference, and artifact burden can affect the covariance structure. Fifth, the results on temporal instability need to be replicated in separate cohorts.

Future work should include testing the system on separate schizophrenia EEG datasets, assessing its robustness to channel montage and preprocessing decisions, and exploring cross-dataset generalization. A fully nested architecture, where recording duration, model hyperparameters, and representation choices are all selected within the outer training data would produce a stronger unbiased estimate of a jointly optimized operating point.

6 Conclusion

We propose a concise covariance-eigenvalue paradigm for subject-independent schizophrenia EEG analysis. The representation was validated over five frequency subbands, recording durations, temporal segments and SVD-derived structural measurements. The prediction capability was tested utilizing strict subject-level LOSO validation. The final locked 10-s five-band representation with XGBoost obtained 89.29% accuracy, 88.97% balanced accuracy, 90.71% ROC-AUC, 93.33% sensitivity and 84.62% specificity.

The combined analyzes reveal that covariance-eigenvalue structure contains group-related information across frequency, temporal and dimensionality viewpoints. Theta and Beta temporal-instability measures survived FDR correction; Alpha $\lambda_1$was the only band-wise eigenvalue comparison surviving FDR; The SVD-derived cumulative-energy ranks and the energy-based measures exhibited corrected group differences .

Table 19 Reproducibility checklist for the final experiment.

Stage	Final implementation
Subject selection	84 subjects; 39 HC and 45 SCZ
Recording	16 channels; 128 Hz; approximately 60 s
Covariance	$R = XX^T/(N-1)$ after channel-wise mean centering
Eigendecomposition	Symmetric eigendecomposition; descending eigenvalue order
Frequency bands	Delta, Theta, Alpha, Beta, Gamma
Final feature vector	80 eigenvalues (5 bands $\times$ 16 eigenvalues)
Final duration	10 s; selected from tested durations
Classifier	XGBoost; fixed configuration
Validation	Strict subject-level LOSO
Uncertainty	10,000 subject-level bootstrap resamples
Paired classifier test	Exact McNemar
Multiple-comparison correction	Holm correction across four classifier comparisons
Interpretability	Global SHAP analysis
Feature-selection sensitivity	Nested SHAP/ANOVA and local $K = 55$–65; not retained
SVD	Structural/interpretive analysis; not independent predictive source

SHAP provided model interpretation, whereas nested feature-selection trials did not improve the full 80-feature representation.
The main contribution is a systematic characterization of the multichannel EEG covariance structure in terms of its eigenvalue spectrum, rather than aiming for absolute state-of-the-art classification accuracy. The final result is still an internal selected-condition estimate and needs independent-cohort validation before any clinical or biomarker claims can be considered.

7 Reproducibility Checklist

The final experimental configuration used to conduct this research is summarized in Table 19. The study involved 84 participants (39 healthy controls and 45 schizophrenia patients) using 16-channel EEG recordings sampled at 128 Hz. After channel-wise mean centering, covariance matrices were constructed and subjected to symmetric eigen decomposition, with eigenvalues arranged in descending order. Features were derived from five frequency bands (delta, theta, alpha, beta, and gamma), resulting in an 80-dimensional covariance-eigenvalue feature vector.A 10-s recording duration and a fixed XGBoost configuration were adopted based on the preceding sensitivity analyses. The effectiveness of the model was assessed by strict subject-level leave-one-subject-out validation, with uncertainty measured through 10,000 bootstrap resamples at the subject level. Statistical comparisons were undertaken using the exact McNemar test with Holm correction, while global SHAP and supplementary SHAP/ANOVA analyzes to evaluate model interpretability and feature selection sensitivity. Thus, Table 19 provides the consolidated implementation details required to reproduce the final experiment.

Declaration

Author Contributions

Ratheesh Sudheerbabu: Conceptualization, Methodology, Software, Writing – original draft, Writing – review & editing. **Abhishek S:** Methodology, Software, Supervision, Validation, Writing – review & editing. **Vinaykumar B:** Review & editing.

Declaration of Competing Interest

The authors declare that they have no known competing financial interests or personal relationships that could have appeared to influence the work reported in this paper.

Acknowledgements

The authors gratefully acknowledge Sri Mata Amritanandamayi Devi (Amma), Chancellor, Amrita Vishwa Vidyapeetham, for her inspiration and for providing financial support for the Article Processing Charges (APC) of this publication.

Data Availability

The dataset analyzed in this study is publicly available. The MSU EEG schizophrenia dataset is available from the M.V. Lomonosov Moscow State University EEG database at http://brain.bio.msu.ru/eeg_schizophrenia.htm. No new human-subject data were collected for this study.

Funding

The authors received no specific funding for this work.

Consent of Participate

Not applicable. This study involved secondary analysis of an existing MSU EEG dataset, and no new participants were recruited

Consent to Publish

Not applicable. This study doesnot report any identifiable individual information.

Ethics Approval

Not applicable. No direct recruitement or intervention with human participants were involved in the study, only secondary computational analysis of an existing dataset was done.

References

[1] Zulqarnain, M., Razzaq, H.H., Gifal, A.S., Aftab, M.N.: An optimized eeg-based hybrid deep learning framework for schizophrenia detection. Biomedical Engineering Letters, 1–15 (2025)

[2] Ali, S., Parveen, S., Khan, I.R., Alankar, B.: Schizophrenia detection using distributed activation function-based statistical attentional bidirectional-long short-term memory. Computers in Biology and Medicine **186**, 109650 (2025)

[3] Dhongade, D., Captain, K., Dahiya, S.: Eeg-based schizophrenia detection: Integrating discrete wavelet transform and deep learning. Cognitive Neurodynamics **19**(1), 1–17 (2025)

[4] Yasin, S., Adeel, M., Draz, U., Ali, T., Hijji, M., Ayaz, M., Marei, A.M.: A cnn-transformer fusion model for proactive detection of schizophrenia relapse from eeg signals. Bioengineering **12**(6), 641 (2025)

[5] Padayatty, R.V., *et al.*: Detection of schizophrenia using eeg signals: A machine learning approach. In: 2022 International Conference on Futuristic Technologies in Control Systems & Renewable Energy (ICFCR), pp. 1–8 (2022). IEEE

[6] Ranjan, R., Sahana, B.C.: Multiresolution feature fusion for smart diagnosis of schizophrenia in adolescents using eeg signals. Cognitive Neurodynamics **18**(5), 2779–2807 (2024)

[7] Zhu, G., Xu, Q., Zhang, F., Yang, Y., Li, X., Li, B., Li, S.: Schizophrenia identification using machine learning methods with graph-theoretic features. Journal of Shanghai Jiaotong University (Science), 1–10 (2025)

[8] Ranjan, R., Sahana, B.C.: A machine learning framework for automatic diagnosis of schizophrenia using eeg signals. In: 2022 IEEE 19th India Council International Conference (INDICON), pp. 1–6 (2022). IEEE

[9] Alazzaw, A., Aljumaili, S., Duru, A.D., Ucan, O.N., Bayat, O., Coelho, P.J., Pires, I.M.: Schizophrenia diagnosis based on diverse epoch size resting-state eeg using machine learning. PEERJ COMPUTER SCIENCE **10** (2024)

[10] Tyagi, A., Singh, V.P., Gore, M.M.: Detection of schizophrenia from eeg signals using selected statistical moments of mfc coefficients and ensemble learning. Neuroinformatics **22**(4), 499–520 (2024)

[11] Mao, Y., Wang, F., Wang, S., Wang, Z., Li, G., Qi, X., Sun, Y.: Ensemble learning techniques reveals multidimensional eeg feature alterations in pediatric schizophrenia. Frontiers in Human Neuroscience **19**, 1530291 (2025)

[12] Goshvarpour, A.: Enhancing schizophrenia diagnosis through eeg frequency waves and information-based neural connectivity feature fusion. Biomedical Signal

Processing and Control **106**, 107717 (2025)

[13] Latreche, I., Slatnia, S., Kazar, O., Harous, S., Khelili, M.A.: Identification and diagnosis of schizophrenia based on multichannel eeg and cnn deep learning model. Schizophrenia Research **271**, 28–35 (2024)

[14] Barros, C., Silva, C.A., Pinheiro, A.P.: Advanced eeg-based learning approaches to predict schizophrenia: Promises and pitfalls. Artificial intelligence in medicine **114**, 102039 (2021)

[15] Khalfallah, S., Puech, W., Tlija, M., Bouallegue, K.: Exploring the effectiveness of machine learning and deep learning techniques for eeg signal classification in neurological disorders. IEEE Access **13**, 17002–17015 (2025)

[16] Bhadra, S., Kumar, C.J., Bhattacharyya, D.K.: Multiview eeg signal analysis for diagnosis of schizophrenia: an optimized deep learning approach. Multimedia Tools and Applications **84**(24), 27577–27608 (2025)

[17] Siuly, S., Khare, S.K., Bajaj, V., Wang, H., Zhang, Y.: A computerized method for automatic detection of schizophrenia using eeg signals. IEEE Transactions on Neural Systems and Rehabilitation Engineering **28**(11), 2390–2400 (2020)

[18] Nattudurai, N.: Classifying schizophrenia disorder through eeg signal analysis and machine learning. In: 2023 IEEE MIT Undergraduate Research Technology Conference (URTC), pp. 1–4 (2023). IEEE

[19] Hwang, H.-H., Choi, K.-M., Kim, S., Lee, S.-H.: Machine learning-based differentiation of schizophrenia and bipolar disorder using multiscale fuzzy entropy and relative power from resting-state eeg. Translational Psychiatry **15**(1), 144 (2025)

[20] Bose, T., Sivakumar, S.D., Kesavamurthy, B.: Identification of schizophrenia using eeg alpha band power during hyperventilation and post-hyperventilation. Journal of Medical and Biological Engineering **36**(6), 901–911 (2016)

[21] Übeyli, E.D.: Modified mixture of experts employing eigenvector methods and lyapunov exponents for analysis of electroencephalogram signals. Expert Systems **26**(4), 339–354 (2009)

[22] Dovedi, T., Upadhyay, R., Kumar, V.: An explainable ai framework for eeg-based schizophrenia detection using mvmd and phase space dynamics. Computers and Electrical Engineering **138**, 111318 (2026)

[23] Abhishek, S., Kumar, S., Mohan, N., Soman, K.: Eeg based automated detection of seizure using machine learning approach and traditional features. Expert Systems with Applications **251**, 123991 (2024)

[24] Rajendran, R., Menon, K.N., Nair, S.C.: Nanotechnology approaches for enhanced

cns drug delivery in the management of schizophrenia. Advanced Pharmaceutical Bulletin **12**(3), 490–508 (2021)

[25] Bagherzadeh, S., Shahabi, M.S., Shalbaf, A.: Detection of schizophrenia using hybrid of deep learning and brain effective connectivity image from electroencephalogram signal. Computers in Biology and Medicine **146**, 105570 (2022)

[26] Pain, S., Sarma, M., Samanta, D.: Graph signal processing and graph learning approaches to schizophrenia pattern identification in brain electroencephalogram. Biomedical Signal Processing And Control **100**, 106954 (2025)

[27] SJ, J., GS, S., Chandrasekaran, B., Byju, S., P, D.: A comparative evaluation of eeg-based deep learning models for schizophrenia detection with cross-dataset validation and explainable ai. Neurological Research, 1–36 (2026)

[28] Chen, P., Yang, X., Zhang, H., Huang, Y., Feng, H., Wang, Y.: End-to-end eeg-based schizophrenia detection via hybrid temporal–spatial dependency learning. Expert Systems **43**(10), 70424 (2026)

[29] Gashkarimov, V., Sultanova, R., Efremov, I., Asadullin, A.: Machine learning techniques in diagnostics and prediction of the clinical features of schizophrenia: A narrative review. Consortium Psychiatricum **4**(3 (eng)), 43–53 (2023)

[30] Luján, M.Á., Jimeno, M.V., Mateo Sotos, J., Ricarte, J.J., Borja, A.L.: A survey on eeg signal processing techniques and machine learning: Applications to the neurofeedback of autobiographical memory deficits in schizophrenia. Electronics **10**(23), 3037 (2021)